Materials Science-Poland, 36(2), 2018, pp. 327-336
http://www.materialsscience.pwr.wroc.pl/
DOI: 10.1515/msp-2018-0045

DE GRUYTER OPEN

A novel photoelectrode of NiO@ZnO nanocomposite prepared by Pechini method coupled with PLD for efficiency enhancement in DSSCs

AMR A. NADA[1,2], HANAA SELIM[2,*], MIKHAEL BECHELANY[1], MONA EL-SAYED[2], R.M. HEGAZEY[2], EGLAL R. SOUAYA[3], M.F. KOTKATA[4]

[1]Institut Européen des Membranes, UMR 5635, Université Montpellier, CNRS, ENSCM, Place Eugene Bataillon, F-34095 Montpellier cedex 5, France

[2]Egyptian Petroleum Research Institute, 11727, Cairo, Egypt

[3]Chemistry Department, Faculty of Science, Ain Shams University, Cairo 11566, Egypt

[4]Semiconductors Technology Lab., Physics Department, Faculty of Science, Ain Shams University, Cairo 11566, Egypt

The dye-sensitized solar cells made of NiO@ZnO nanoparticles were synthesized by a novel Pechini route using different NiO molar concentration ratios. The thermal, structural morphological, optical and electrical properties of the prepared samples were investigated using thermal gravimetric analysis and differential scanning calorimetery (TGA/DSC), X-ray diffraction (XRD), high-resolution transmission electron microscopy (HR-TEM), FT-IR and Raman spectroscopy, UV-diffuse reflectance (UV-DRS), photoluminescence (PL) and current-voltage (I-V) measurements. The success of doping process was confirmed by the XRD patterns, which revealed the existence of new peak at 43.2° corresponding to secondary phase NiO. UV spectra exhibited red shifts in NiO doped ZnO NCs and PL spectra showed strong emission band at 355 nm. The doping of ZnO with NiO was intended to enhance the surface defects of ZnO. The current-voltage measurements showed an improvement of the short circuit photocurrent (J_{sc}) and fill factor (FF) and a decrease in the open circuit voltage (V_{OC}) for dye-sensitized solar cell (DSSC) based on NiO–ZnO NCs. A clear enhancement in efficiency of DSSC from 1.26±0.10 % for pure ZnO to 3.01±0.25 % for NiO–ZnO NCs at the optimum doping with 1.5 mol% of NiO to ZnO (ZN1.5) was observed. The obtained material can be a suitable candidate for photovoltaic applications.

Keywords: *ZnO nanoparticles; NiO/ZnO nanocomposite; dye-sensitized solar cell (DSSC); efficiency*

1. Introduction

In recent years, nano-metal-oxide semiconductors have gained a great interest in optoelectronics and photovoltaics due to their electrical, optical and chemical properties [1, 2]. Doped zinc oxide (ZnO) has been a subject of many studies because of its potential for important applications such as those in optoelectronic and luminescent devices [3], heterojunction solar cells [4], transparent conductors [5], and chemical and gas sensors [6, 7]. ZnO has unique structural, electrical, and optical properties, wide energy band gap (3.37 eV) and large exciton binding energy (60 meV). Therefore, ZnO was considered as a potential candidate for electronic and optoelectronic applications such as photonic crystals, light-emitting diodes, sensors, electro- and photoluminescent materials [8]. ZnO nanoparticles can be prepared on a large scale at low cost by simple solution based methods, such as chemical precipitation, sol-gel synthesis, and hydrothermal reaction [9–11].

In addition to these applications, ZnO also shows its potentiality in dye sensitized solar cells (DSSCs). DSSCs are a new type of metal oxide wide-band-gap solar cells composed of a semiconductor photoanode absorbing dye molecules, a counter electrode, and an electrolyte between the photoanode and counter electrode. In recent years, dye sensitized titanium dioxide (TiO_2) solar cell made by O'Regan et al. [42] has been

*E-mail: hanaaselimali@yahoo.com

considered as a cost-effective alternative to traditional solar cells. Nowadays, the ZnO DSSC modified with other semiconductor materials have been widely investigated to improve the cell performance [12–15].

Several reports were focused on optimizing and enhancing optical, electrical and magnetic properties of ZnO by doping with transition metals such as Cu, Co, Ni, Ti, Au, Co, etc. [16], which created new materials with potential application in semiconductor devices. Among promising dopants, nickel oxide is considered as a model p-type semiconductor with a wide band gap energy ranging from 3.6 eV to 4.0 eV. Thus, it has a wide range of applications such as smart windows, spin valves, giant magnetoresistance (GMR) sensors, solar cells, etc. [17]. Doping NiO with ZnO nanoparticles results in a drastic and interesting change in the optical, electrical, and magnetic properties [18].

In this work, NiO doped ZnO NCs were successfully synthesized by a novel Pechini route with different molar concentrations of zinc nitrate and nickel nitrate as chelating materials and citric acid and ethylene glycol as connecting materials. The structural, morphological, thermal, optical and electrical properties of NiO doped ZnO NCs were studied using X-ray diffraction (XRD), high-resolution transmission electron microscopy (HR-TEM) , thermal gravimetric analysis (TGA), FT-IR and Raman spectroscopy, UV-diffuse reflectance (UV-DRS), photoluminescence (PL). The performance of DSSC was investigated by I-V measurements.

2. Materials and method

2.1. Materials

All chemicals used were reagents of analytic grade. Zinc nitrate ($Zn(NO_3)_2{\cdot}6H_2O$) (228737, 98 %), nickel nitrate ($Ni(NO_3)_2{\cdot}6H_2O$) (72252, >98.5 %), citric acid monohydrate ($C_6H_8O_7{\cdot}H_2O$) (1909, >99 %), ethylene glycol ($HOCH_2CH_2OH$) (1.00949, >99 %), lithium iodide (LiI) (223816, 98 %), eosin-Y (230251) and hydrogen hexachloroplatinate (IV) hexahydrate ($H_2PtCl_6.6H_2O$) (81080, 38 %) were obtained from Sigma-Aldrich Company. Iodine (I_2) (13380, 99.8 %), ethanol (02875, 99.8 %) and acetone (179973, 99.5 %) were obtained from Honeywell Company.

2.2. Preparation of NiO doped ZnO NCs

ZnO nanoparticles were synthesized by co-precipitation method [19]. Typically, 7.44 mg of zinc nitrate $Zn(NO_3)_2$ was dissolved in 500 mL deionized water and stirred for 30 minutes at 100 °C. The pH was adjusted at 6 using 1 M NaOH and stirring it for one hour. The mixture was centrifuged at a speed of 4000 rpm and the precipitates were collected. The white powder obtained was washed several times with deionized water and ethanol. It was then dried at 80 °C in an electric oven and calcinated at 450 °C for 4 hours in the air to remove any organic residues.

NiO doped ZnO NCs were prepared by Pechini method with different molar ratios (0.5 %, 1.0 %, 1.5 %, 2.0 % and 2.5 %) of NiO precursor, as shown schematically in Fig. 1, and labeled as (ZN0.5, ZN1.0, ZN1.5, ZN2.0 and ZN2.5). Citric acid monohydrate ($C_6H_8O_7{\cdot}H_2O$) and ethylene glycol ($HOCH_2CH_2OH$) were dissolved completely in deionized water to form a sol at 60 °C for 1 h in oil bath, and further heated at 80 °C for 1 h to remove excess of water. The reagents Zn $(NO_3)_2{\cdot}6H_2O$ and Ni $(NO_3)_2{\cdot}6H_2O$ were added to the solution and heated at 110 °C for 1 h in order to start esterification. The green solution became more and more viscous and finally a xerogel was obtained. The xerogel was dried at 80 °C for 24 h in an electric oven, and then it was pyrolyzed at 450 °C for 4 h in nitrogen. The obtained powders were calcinated at different temperatures (400 °C, 600 °C and 800 °C) for 4 h, then they were ball milled for 30 min to break down the agglomerates.

2.3. Fabrication of DSSC electrodes

All the considered samples were deposited on quartz substrates coated with indium tin oxide (ITO) with a thickness of 100 nm to 150 nm using pulse laser deposition (PLD) method

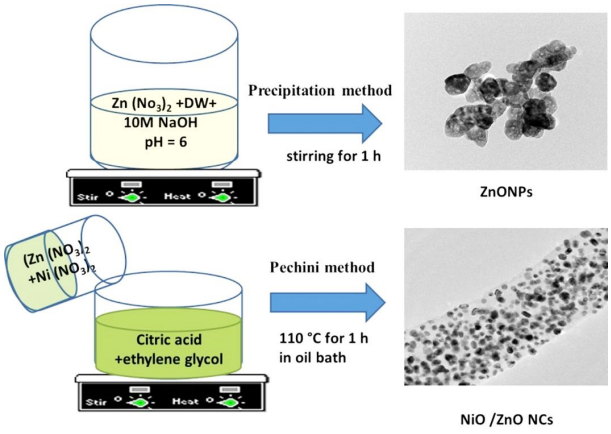

Fig. 1. Preparation of pure ZnO nanoparticles and ZnO doped with NiO nanocomoposites.

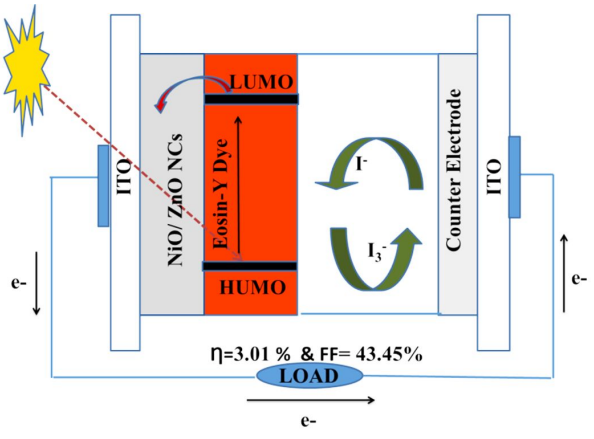

Fig. 2. Schematic diagram of dye sensitized solar cell.

at a wavelength of 1064 nm (Q-switched Nd:YAG laser). The prepared thin films were used as photoelectrodes for DSSCs. The prepared photoelectrodes were immersed in 0.04 g of eosin-Y organic dye ($C_{20}H_8Br_4Na_2O_5$) dissolved in 100 mL acetone for 24 hours. The platinum-coated counter electrode was prepared from 4 mM hydrogen hexachloroplatinate(IV) hexahydrate ($H_2PtCl_6.6\ H_2O$) in ethanol solution, deposited on ITO-glass and calcined at 400 °C in air for 1 h. The redox electrolyte consisting of 0.3 M LiI and 0.03 M I_2 in polyethylene carbonate was injected into the inter-electrode space from the counter electrode side through a predrilled hole as shown in Fig. 2.

3. Experimental

The differential thermal analysis was carried out using Q600 DST-DSC/TGA apparatus at a heating rate of 10 °C/min in the temperature range from room temperature to 1000 °C under air flow. The phase of the prepared samples was examined by X-ray diffraction (XRD) using a diffractometer (PANalytical X'Pert PRO MPD). CuKα radiation ($\lambda = 1.5418$ Å) was used at 40 kV and 40 mA. The morphology was investigated by high resolution transmission electron microscope (HR-TEM), model JEM-2100, JEOL, Japan. The structural study of the prepared samples was performed by Raman spectroscopy with a laser source of 532 nm and power 10 mW (model Sentera, Bruker, Germany). The functional groups were identified using a Fourier transform infrared spectrometer (FT-IR) model spectrum one (Perkin Elmer, USA) in the wavenumber range of 400 cm^{-1} to 4000 cm^{-1}. The optical reflectance was recorded using a UV-Vis spectrometer (PerkinElmer Lambda 1050). The photoluminescence spectra were recorded using a PerkinElmer LS 50B luminescence spectrophotometer. Photocurrent voltage characteristics were measured using solar simulator Science Tech SS150W-AAA with a xenon lamp as a light source. The cell was exposed to light of intensity 1 Sun (100 mW/cm^2) using AM 1.5 G. I-V tester is 2400 Keithley source meter SSIVT-60WC. In order to calculate the error, the measurement was repeated three times.

4. Results and discussion

4.1. Thermal analysis

The thermal gravimetric analysis and differential scanning calorimeter (TGA/DSC) curves obtained for NiO doped ZnO NPs are shown in Fig. 3. The curve shows two stages of sample degradation. The first stage is observed in the temperature range 26 °C to 125 °C with maximum at 60 °C. It is accompanied by a mass loss of about 4.6 % which is attributed to the evaporation of H_2O. The second stage, observed at the temperature range of 200 °C to 800 °C with maximum at 400 °C, is

exothermic. It is accompanied by a mass loss of about 78.16 % which is attributed to the decomposition and combustions of organic residues. At this stage, the NiO–ZnO composites transformation is complete.

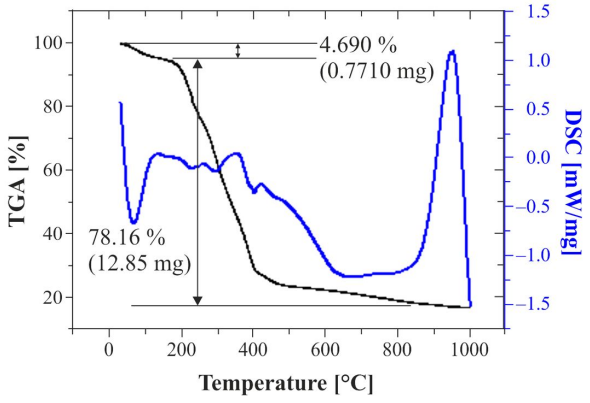

Fig. 3. TGA-DSC curves of ZnO doped with NiO NPs as recorded at a constant heating rate of 10 °C/min.

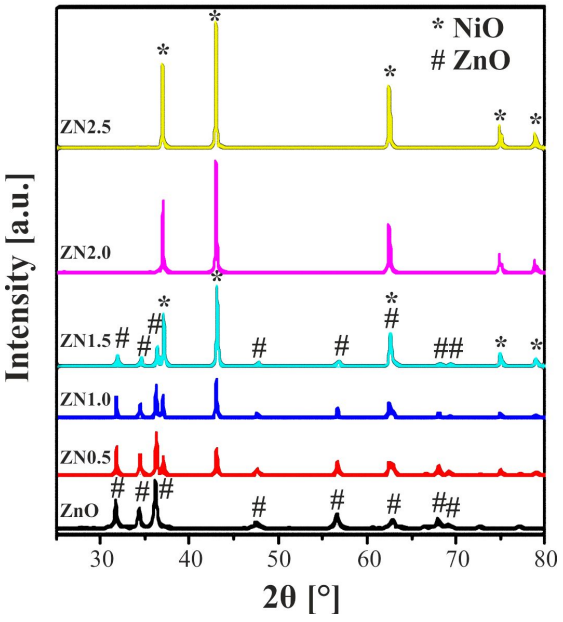

Fig. 4. XRD spectra of ZnO and ZnO doped with NiO at different molar ratios.

4.2. Structural morphological characterization

4.2.1. X-ray diffraction analysis (XRD)

The crystalline phase of all prepared samples was determined by X-ray diffraction. The XRD patterns of ZnO, ZN0.5, ZN1.0, ZN1.5, ZN2.0 and ZN2.5 are presented in Fig. 4. It can be seen that ZnO has peaks that can be well indexed to hexagonal wurtzite structure of zinc oxide NPs (JCPDS Card No. 01-080-4199) with the planes (1 0 0), (0 0 2), (1 0 1), (1 0 2), (1 1 0), (1 0 3), (2 0 0), and (1 1 2) at 31.71°, 34.37°, 36.18°, 47.55°, 56.59°, 62.84°, 67.90° and 68.96°. The intensity of NiO peak increases with increasing the amount of NiO. At higher molar ratio (>1.5) the peaks of ZnO disappear and all observed peaks can be ascribed to high intensity of NiO. The peaks at 2θ = 37.14°, 43.13°, 62.56°, 74.93° and 78.91° are referred to NiO and correspond to the planes (1 1 1), (2 0 0), (2 2 0), (3 1 1) and (2 2 2), respectively, which are indexed to JCPDS Card No. 04-005-9695.

The crystallite size in the samples was calculated from the full width at half maximum (FWHM) of the XRD pattern Fig. 5, using Williamson-Hull formula [20]:

$$\beta \times cos\theta = (K \times \lambda / D) + (4 \times S \times \sin\theta) \qquad (1)$$

where β is FWHM in radians, λ is wavelength of X-ray used, θ is the Bragg scattering angle, D is particle diameter, and S is the strain. The parameter K is the shape factor (taken as 0.94). The calculated particle sizes for the prepared samples are listed in Table 1, and the results indicate that the particle sizes increase with increasing the amount of NiO. Fig. 5 shows the most intense XRD peaks of ZnO and NiO doped ZnO NCs at molar ratio of 1.5 % calcined at 800 °C. As shown, the peak of NiO doped ZnO shifted towards higher angle compared to ZnO and are attributed to the difference between the ionic radii of the elements ($rZn^{2+} = 0.60$ Å and $rNi^{2+} = 0.55$ Å) [21], which indicates that NiO was successfully doped on ZnO.

4.2.2. Transmission electron microscope (TEM) studies

Fig. 6 shows the morphological characterizations of the prepared samples investigated by HR-TEM. It can be seen that the high-purity nanoparticles of mostly spherical regular shapes

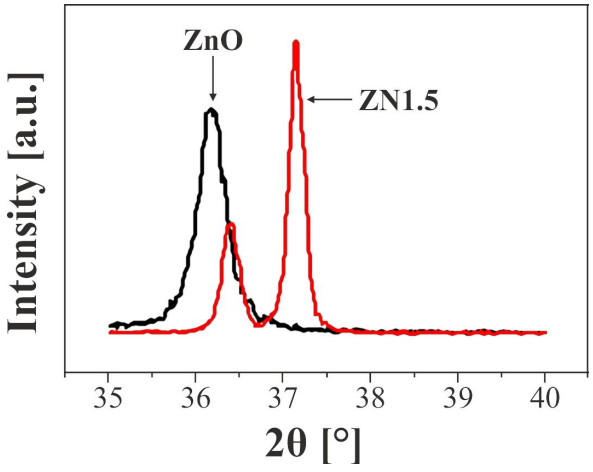

Fig. 5. Displacement of the most intense peak of the XRD pattern provoked by the insertion of Ni and Zn into the crystalline lattice.

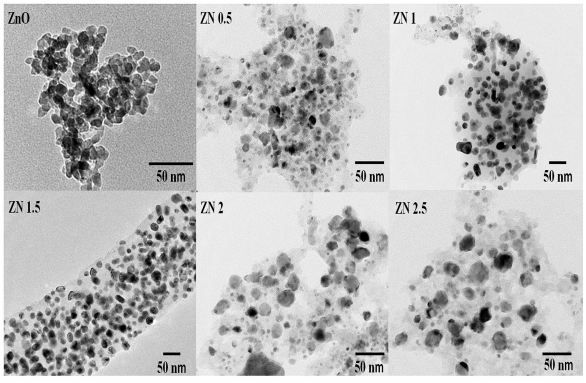

Fig. 6. HR-TEM images of ZnO and ZnO doped with NiO at different molar ratios.

appeared for NiO doped ZnO NCs with different molar ratios from 0.5 % to 2.5 %. The ZnO NPs show hexagonally shaped nanoparticles and larger rectangular platelets. The optimum regular spherical shapes and uniform particle size distribution was obtained for ZN1.5 sample. The particle diameters were measured from the TEM images using image analysis software (Image J1.50i). The average diameter was obtained from 100 measurements of randomly chosen nanoparticles of each sample (Fig. 6). After calcination, we measured average diameters of 9 nm ± 5 nm, 10 nm ± 2 nm, 16 nm ± 2 nm, 24 nm ± 2 nm, 25 nm ± 2 nm and 26 nm ± 2 nm for samples ZnO, ZN0.5, ZN1, ZN1.5, ZN2 and ZN2.5, respectively.

4.2.3. Fourier transform-infrared (FT-IR) spectra

The doping process was successfully confirmed by FT-IR spectra recorded in the range of 400 cm^{-1} to 4000 cm^{-1} for the prepared samples as shown in Fig. 7. The broad absorption peak was observed at around 3367 cm^{-1} corresponding to O–H stretching. The peaks at 1560 cm^{-1} and 1395 cm^{-1} are attributed to the symmetric and asymmetric C=O stretching vibration modes, whereas the small peak at 913 cm^{-1} is attributed to C–H stretching. The peak observed at 430 cm^{-1} is attributed to the stretching mode of Zn–O bond. The spectra of NiO–ZnO NCs show a new vibration mode at 513 cm^{-1} corresponding to Ni–O stretching bond, which indicates that NiO was successfully doped into ZnO NPs. Hence, it is a nice supporting result for the previous investigations.

4.2.4. Raman spectroscopy

Raman spectroscopy shows the vibrational modes of the prepared samples for detecting the incorporation of dopant. As shown in Fig. 8, the spectrum of pure ZnO exhibits a significant peak of E_2 (high) mode at 435 cm^{-1} representing wurtzite hexagonal structure of ZnO associated with the motion of oxygen atoms in ZnO lattice [20] and other peaks observed at 322 cm^{-1}, 578 cm^{-1}, 1130 cm^{-1}, 1368 cm^{-1} and 1525 cm^{-1}. The two peaks at 322 cm^{-1} and 578 cm^{-1} are assigned to be E_{2H}-E_{2L} and A_1 (LO), respectively. The Raman spectra of NiO–ZnO NCs are blue shifted compared to ZnO. The intensity of peak at 435 cm^{-1} decreased, whereas the intensities of peaks at 578 cm^{-1} and 1130 cm^{-1} increased. The peaks at 1368 cm^{-1} and 1525 cm^{-1} vanished with the increasing doping content. According to literature, the additional modes are induced by host lattice defects; the host lattice defects in ZnO are activated and observed with doping content which results in the appearance of these modes [22]. The changes in the intensity of the peaks confirm the successful doping of ZnO.

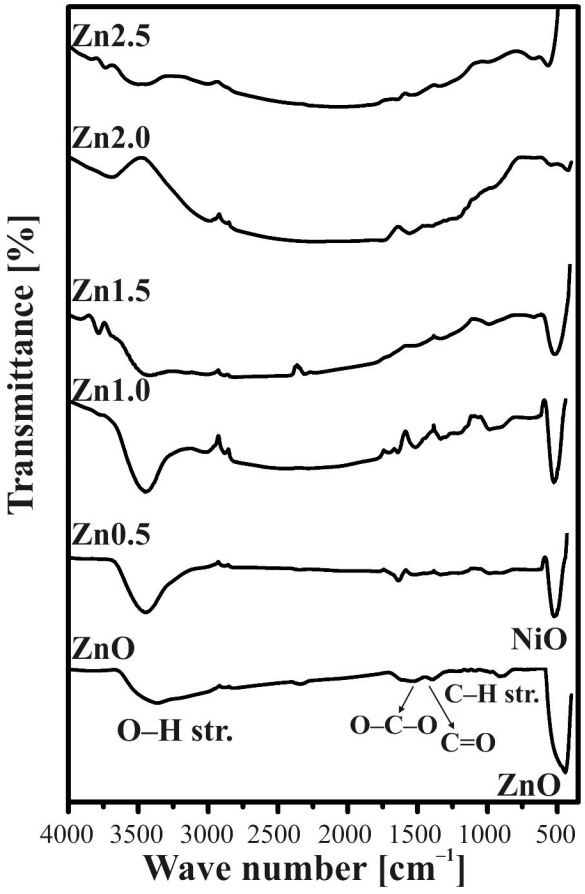

Fig. 7. FT-IR spectra of ZnO and ZnO doped with NiO at different molar ratios.

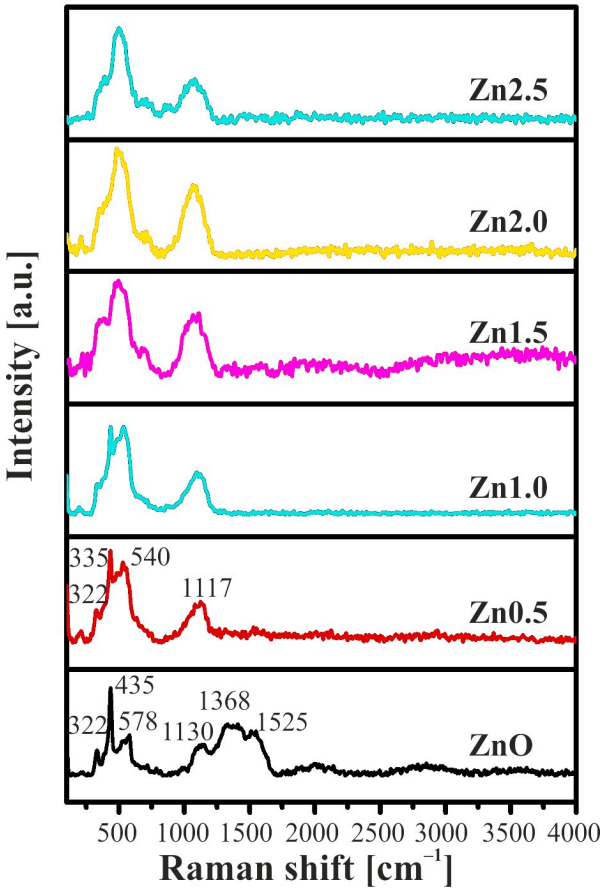

Fig. 8. Raman spectra for the undoped and NiO doped ZnO NPs at different molar ratios.

4.3. Optical characteristics

4.3.1. UV-Vis spectra analysis

Diffuse reflectance spectra of the prepared samples were investigated using UV-Vis optical spectroscopy in the range of 200 nm to 800 nm. As shown in Fig. 9, the values of optical band gaps of the prepared samples have been estimated from the plots of reflection percentage versus energy hυ and tabulated in Table 1. The results indicate that the band gap energies of the prepared doped samples decrease with the increasing amount of dopant up to 2.0 mol%. The band gap of the sample containing 2.5 mol% has been slightly increased in comparison to ZN2. This could be attributed to the quantum confinement effect and the blocking of the low energy transitions by the donor electrons occupying the states at the bottom of the conduction band [23]. The reflectance spectrum of ZnO was studied at 370 nm and a shift towards longer wavelength region for doped ZnO was observed. Hence, the observed red shift in the absorption band may be attributed to the sp-d exchange interactions between the ZnO band electrons and the localized d-electrons of the doped NiO corresponding to d-d transition bands which cause the change in the band structure [24]. The red shift in the band edge with the increasing nickel oxide dopant is a clear indication of the doping of NiO with ZnO [25]. The schematic diagram of the energy band structure of NiO doped with ZnO is shown in Fig. 10, where the electrons in the valence bands (VB) could be excited to the conduction bands (CB) with simultaneous generation of the same amount of holes in the VB. Meanwhile, the electron transfer occurs from ZnO to

NiO, and the hole transfer occurs from NiO to ZnO until the system attains equilibrium due to the carrier diffusion between the NiO and ZnO. The charge carrier separation leads to an increase in the carrier lifetime and enhances the absorption efficiency. The preliminary results show an evident enhancement of the ability of NiO doped ZnO NCs to harvest UV light.

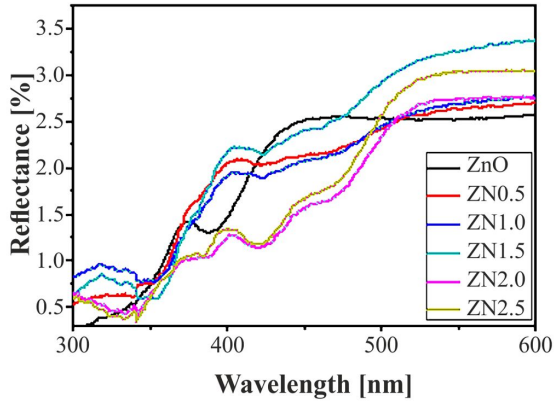

Fig. 9. UV-Vis diffuse reflectance spectra of ZnO and ZnO doped with NiO at different molar ratios.

Table 1. Average crystal size D and energy band gap Eg of ZnO and NiO doped ZnO NPs.

NiO Conc. [%]	D [nm]	E_g [eV]
ZnO	26	3.32
ZN0.5	48	3.26
ZN1.0	59	3.22
ZN1.5	78	3.11
ZN2.0	91	3.09
ZN2.5	74	3.10

4.3.2. Photoluminescence (PL) spectroscopy

The room-temperature PL spectra of the investigated samples at excitation wavelength of 325 nm are shown in Fig. 11. The UV emission is attributed to the near-band-edge emission caused by the recombination of free excitons through an exciton-exciton collision process [26, 27]. The PL spectrum of pure ZnO reveals strong and broad UV band peak centered at 354 nm. After NiO doping,

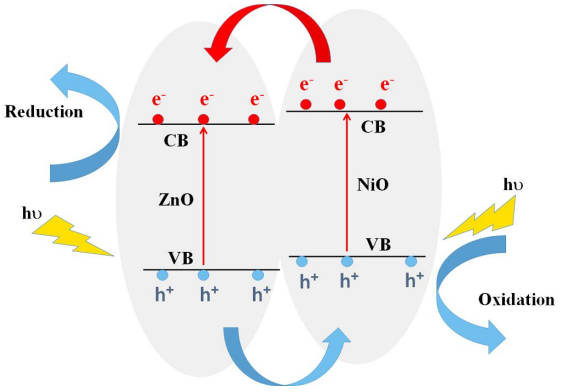

Fig. 10. The diagram of the energy band structures of NiO doped with ZnO.

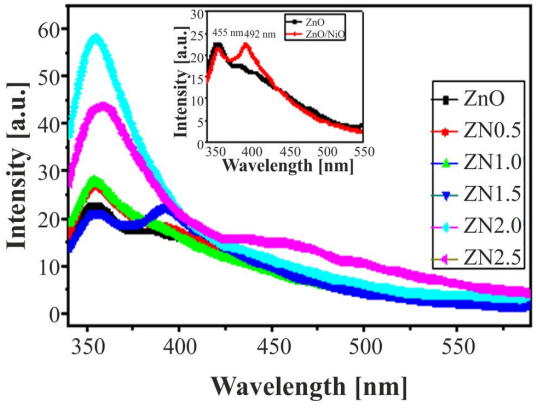

Fig. 11. Photoluminescence spectra of ZnO and ZnO doped with NiO at different molar ratios.

the UV emission peaks shift to a wavelength at 355 nm, and the intensity of UV peaks decreases indicating low recombination between electrons and holes. The blue shift of the UV emission peak can be attributed to the strong interaction between the d-electrons of NiO and the s, p electrons of the host band. The optimum doping was observed for ZN1.5, which shows multi-emission centers at 355 nm and 392 nm. These results show a great potential of the NiO doped ZnO NCs in optoelectronics devices.

4.4. Current-voltage characteristics

Current-voltage (I-V) characteristics curves of DSSC based on ZnO NPs and DSSC based on

Table 2. DSSC PV parameters at different NiO@ZnO mol%.

NiO@ZnO [mol%]	0.0	0.5	1.0	1.5	2.0	2.5
J_{SC} [mA·cm^{-2}]	0.82	1.24	1.42	1.94	2.39	2.45
V_{OC} [V]	0.47	0.37	0.36	0.35	0.21	0.21
FF [%]	32.25	37.56	39.72	43.45	36.73	35.69
η [%]	1.26±0.10	1.75±0.14	2.08±0.17	3.01±0.25	1.91±0.16	1.84±0.15

Table 3. Photovoltaic parameters of the DSSCs from previous and present work.

Sample name	J_{SC} [mA·cm^{-2}]	V_{OC} [V]	FF [%]	η [%]	Literature
Urchin ZnO nanowires (U-ZnO NWs)	0.00	0.10	4.0	0.00	[33]
U-ZnO NWs/10 nm TiO_2 ALD layer	0.34	0.76	55.0	0.28	[33]
U-ZnO NWs/TiO_2 NPs (10 μm)	2.03	0.64	59.0	1.50	[33]
U-ZnO NWs/10 nm TiO_2 ALD layer + TiO_2 NPs (10 μm)	2.64	0.68	50.0	1.80	[33]
ZnO nanowires	2.11	0.40	51.5	0.43	[34]
ZnO hierarchical microspheres	5.15	0.53	61.5	1.67	[34]
ZnO–TiO_2 seed layer	2.25	0.52	48.0	0.56	[35]
ZnO nanowire	3.12	0.54	50.0	0.84	[35]
ZnO nanowires	2.37	0.64	49.8	0.75	[36]
ZnO branched nanowires	4.27	0.68	52.2	1.51	[36]
TiO_2–ZnO thin film	2.52	0.74	43.0	0.79	[37]
ZnO nanorods@TiO_2–ZnO	7.92	0.62	37.0	1.81	[37]
Cd:ZnO@TiO_2 (core-shell):Mg	1.00	0.73	58.4	0.48	[38]
ZnO nanowire@ZnO–TiO_2	2.53	0.77	33.0	0.64	[39]
ZnO nanowire with 0.1 % PVA@ZnO–TiO_2	2.69	0.75	41.0	0.82	[39]
ZnO with oxygen plasma treatment	1.10	0.42	43.0	0.76	[40]
NiO	1.38	0.08	34.1	0.04	[41]
0.5 % Li-doped NiO	1.49	0.08	35.1	0.04	[41]
1 % Li-doped NiO	1.66	0.09	35.2	0.05	[41]
2 % Li-doped NiO	1.19	0.09	36.5	0.04	[41]
1.5 mol% NiO@ZnO	1.94	0.35	43.5	3.01	Present work

NiO doped ZnO NCs are shown in Fig. 12a, and the detailed photovoltaic (PV) parameters obtained from I-V curves as a function of NiO precursor amount are summarized in Table 2. For comparison, the performance of ZnO DSSC and NiO–ZnO DSSC reveals an improvement in the short circuit photocurrent (J_{sc}) from 0.82 mA/cm^2 to 2.45 mA/cm^2, fill factor (FF) from 32 % to 43 % and a decrease in the open circuit voltage (V_{OC}) from 0.47 V to 0.21 V. Fig. 12b shows the variation of the efficiency η with NiO precursor amount. The results indicate a clear enhancement in efficiency from 1.26±0.10 % for the ZnO based cell to 3.01±0.25 % for ZN1.5 due to the creation

of energy barrier which reduces the rate of electron recombination back to dye molecules and electrolyte species [28–30]. The decrease in efficiency with further doping can be attributed to the decrease of dye-adsorption efficiency of the ZnO film due to screening by larger amount of dopant [31]. Hence, the light harvesting rate and the electron injection rate will, consequently, decrease and this will be reflected by the decrease of both J_{SC} and η [32]. The obtained results show that the doping of ZnO with NiO leads to enhancement in the efficiency of NiO–ZnO cell, which is characterized by excellent long-term stability and can be a suitable candidate for commercial DSSC applications [33]. The DSSC efficiency of ZN1.5 is notably higher as compared with the efficiency obtained in previous reports as presented in Table 3 [33–41].

5. Conclusions

NiO doped ZnO NCs were synthesized by a novel Pechini route with different precursor molar ratios from 0.0 mol% to 2.5 mol% using citric acid and ethylene glycol. The structural, morphological, thermal, optical and electrical characterizations were carried out. The success of the doping process was confirmed by the XRD patterns which showed the existence of a new peak at 43.2° at (2 0 0) plane corresponding to secondary phase NiO. XRD study also showed that the optimum molar concentration ratio is 1.5 mol%. FT-IR spectra revealed the presence of a new vibration mode at 513 cm^{-1} corresponding to NiO stretching mode in NiO–ZnO NCs. Raman spectra showed blue shifting to lower frequencies due to the increase of the doping content. UV spectra showed red shifts in the absorption band edge upon the NiO doping. PL spectra revealed the reduction of recombination between h^+/e^- in ZN1.5 sample. The current-voltage characteristics showed a clear enhancement in efficiency of the cell based on ZnO from 1.26±0.10 % for pure to 3.01±0.25 % for NiO doped at the optimum molar ratio of 1.5 (ZN1.5). This cell can be a suitable candidate for photovoltaic applications.

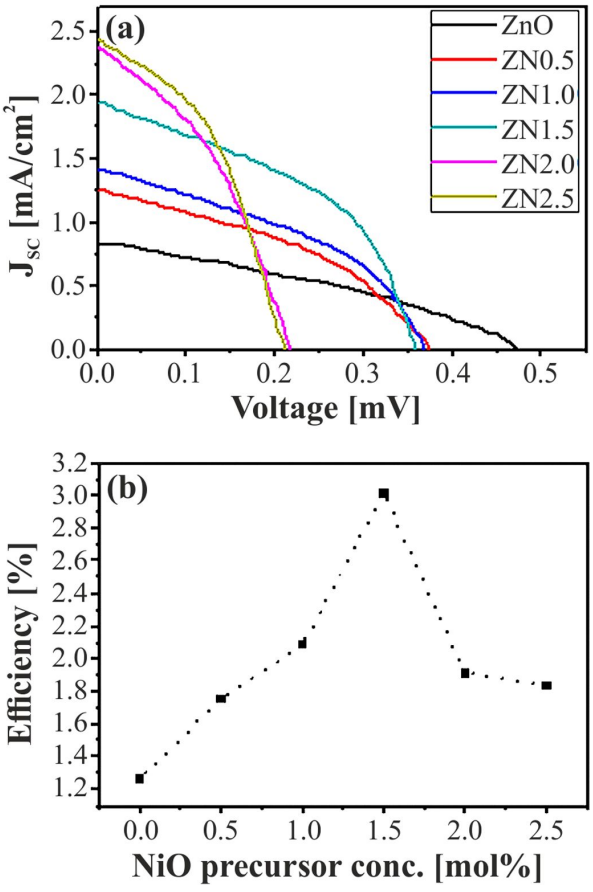

Fig. 12. I-V characteristics of ZnO and NiO–ZnO based DSSC and (b) variation of η with NiO concentration (mol%).

References

[1] Mythili N., Arulmozhi K., *J. Appl. Phys. A,* 118 (2015), 261.

[2] El-Maghrabi H.H., Nada E.A., Soliman F.S., Moustafa Y.M., Amin A. E.S., *Egypt. J. Petrol.,* 25 (2016), 575.

[3] Miyake A., Kominami H., Tatsuoka H., Kuwabara H., Nakanishi Y., Hatanaka Y., *J. Cryst. Growth,* 214 (2000), 294.

[4] Song D., Aberle A.G., Xia J., *J. Appl. Surf. Sci.,* 195 (2002), 291.

[5] Martinez M., Herrero J., Gutierrez M., *Sol. Energ. Mat. Sol. C,* 45 (1997), 75.

[6] Cheng X., Zhao H., Huo L., Gao S., Zhao J., *Sensor. Actuat. B-Chem,* 102 (2004), 248.

[7] Drobek M., Kim J.H., Bechelany M., Vallicari C., Julbe A., Kim S.S., *Acs Appl. Mat. Int.,* 8 (2016), 8323.

[8] Chung T., Luo L., He Z., Leung Y., Shafiq I., Yao Z., *Appl. Phys. Lett.,* 91 (2007), 233112.

[9] ZHANG H., YANG D., MA X., JI Y., XU J., QUE D., *Nanotechnology,* 15 (2004), 622.
[10] ZHANG J., SUN L., YIN J., SU H., LIAO C., YAN C., *Chem. Mater.,* 14 (2002), 4172.
[11] LI W.J., SHI E.W., ZHENG Y.Q., YIN Z.W., *Mater. Sci. Lett.,* 20 (2001), 1381.
[12] KIM S.S., YUM J.H., SUNG Y.E., *J. Photoch. Photobio. A*, 171 (2005), 269.
[13] JOSHI S., MUDIGERE M., KRISHNAMURTHY L., SHEKAR G., *Chem. Pap.,* 68 (2014), 1584.
[14] REN J., QUE W., YIN X., HE Y., JAVED H.A., *RSC Adv.,* 4 (2014), 7454.
[15] FENG Y., CHEN J., HUANG X., LIU W., ZHU Y., QIN W., *Cryst. Res. Technol.,* 51(2016), 548.
[16] FARHA A., MANSOUR S.A., KOTKATA M., *J. Mater. Sci.,* 51 (2016), 9855.
[17] GOKUL B., MATHESWARAN P., ABHIRAMI K., SATHYAMOORTHY R., *Non-Cryst. Solids,* 363 (2013), 161.
[18] HUSAIN S., RAHMAN F., ALI N., ALVI P., *Optoelectron. Eng.,* 1 (2013), 28.
[19] SHALAN A., OSAMA I., RASHAD M., IBRAHIM I., *J. Mater. Sci.-Mater. El.,* 25 (2014), 303.
[20] MEAD D. WILKINSON G., *J. Raman Spectrosc.,* 6 (1977), 123.
[21] EKAMBARAM S., *J. Alloy. Compd.,* 390 (2005), L4.
[22] DUAN L., RAO G., WANG Y., YU J., WANG T., *Appl. Phys.,* 104 (2008), 013909.
[23] LU J., FUJITA S., KAWAHARAMURA T., NISHINAKA H., KAMADA Y., OHSHIMA T., *J. Appl. Phys.,* 101 (2007), 083705.
[24] ZHANG Y., WANG Z., CAO J., *Appl. Phys.,* 113 (2013), 203913.
[25] SHARMA P.K., DUTTA R.K., PANDEY A.C., *J. Magn. Magn. Mater.,* 321 (2009), 3457.
[26] SCHWARTZ D.A., KITTILSTVED K.R., GAMELIN D.R., *Appl. phys. letters.,* 85 (2004), 1395.
[27] VITER R., IATSUNSKYI I., FEDORENKO V., TUMENAS S., BALEVICIUS Z., RAMANAVICIUS A., *J. Phys. Chem. C,* 120 (2016), 5124.
[28] LIU Y., SUN X., TAI Q., HU H., CHEN B., HUANG N., *J. Power Sources,* 196 (2011), 475.
[29] KAO M., CHEN H., YOUNG S., *J. Appl. Phys. A,* 97 (2009), 469.
[30] KIM S.S., YUM J.H., SUNG Y.E., *Sol. Energ. Mat. Sol. C,* 79 (2003), 495.
[31] AL-JUAID F., MERAZGA A., *Energ. Power Eng.,* 5 (2013), 591.
[32] SOGA T., *Nanostructured materials for solar energy conversion*, Elsevier, Nagoya, Japan, 2006.
[33] KARAM C., GUERRA-NUÑEZ C., HABCHI R., HERRO Z., ABBOUD N., KHOURY A., *Mater. Design,* 126 (2017), 314.
[34] KANG X., JIA C., WAN Z., ZHUANG J., FENG J., *RSC Adv.,* 5 (2015), 16678.
[35] MARIMUTHU T., ANANDHAN N., THANGAMUTHU R., MUMMOORTHI M., RAVI G., *J. Alloy. Compd.,* 677 (2016), 211.
[36] CHENG H.M., CHIU W.H., LEE C.H., TSAI S.Y., HSIEH W.F., *J. Phys. Chem. C,* 112 (2008), 16359.
[37] MARIMUTHU T., ANANDHAN N., *Mater. Res. Bull.,* 95 (2017), 616.
[38] AKO R.T., PEIRIS D., EKANAYAKE P., TAN A.L., YOUNG D.J., ZHENG Z., *Sol. Energ. Mat. Sol. C,* 157 (2016), 18.
[39] MARIMUTHU T., ANANDHAN N., THANGAMUTHU R., SURYA S., *Superlattice. Microst,* 98 (2016), 332.
[40] KHADTARE S., BANSODE A.S., MATHE V., SHRESTHA N.K., BATHULA C., HAN S.H., *J. Alloy. Compd.,* 724 (2017), 348.
[41] WEI L., JIANG L., YUAN S., REN X., ZHAO Y., WANG Z., *Electrochim. Acta,* 188 (2016), 309.
[42] O'REGAN B., GRÄTZEL M., *Nature*, 353 (1991), 737.

Received 2017-12-27
Accepted 2018-03-20